Anthropomorphic head phantom for quantitative image quality assessment in cone beam computed tomography using materials for 'home made' fabrication techniques

Y. Wang[a,*]

[a]*Department of Biomedical Engineering, Delft University of Technology, Delft, the Netherlands*

Abstract

Introduction: In this study, a novel anthropomorphic head phantom for quantitative image quality assessment in cone beam computed tomography (CBCT) is proposed. The phantom is composed of tissue equivalent materials (TEMs) which are suitable for 'home made' fabrication methods such as silicone casting and 3D printing and equipped with inserts for quantitative measurement of the contrast resolution. A monocalcium phosphate/gypsum mixture (MCPHG), nylon and a silyl modified polymer gel (SMP) are proposed as bone, muscle and brain equivalent materials respectively. **Methods:** The TEMs within a prototype were evaluated for their radiodensity in terms of Hounsfield Units (HU). Separate TEM samples were evaluated for their scatter magnitude and spatial distribution. The measurements were compared with theoretical HU values and Monte Carlo based scatter simulations of bone, muscle and brain tissue. **Results:** The median radiodensity and inter quartile range (IQR) of the MCPHG and SMP were found to be within the range of the theoretical radiodensity for bone and brain tissue: 922 (IQR = 156) and 47 (IQR = 7) HU respectively. The median radiodensity of nylon was slightly outside of the HU range of muscle tissue, but within the HU range of a combination of muscle and adipose tissue: -18 (IQR = 40) HU. The median ratios between the measured scatter characteristics and simulated tissues were between 0.84 and 1.13 after removal of one outlier (IQR between 0.05 and 0.14). **Conclusions:** The preliminary results of this study show that the proposed design and TEMs are potentially suitable for the fabrication of a 'home made' anthropomorphic head phantom for quantitative image quality assessment in CT or CBCT.

Keywords
Anthropomorphic Head Phantom, Tissue Equivalent Materials, Cone Beam Computed Tomography, Radiodensity, Scatter

1. Introduction

Cone beam computed tomography (CBCT) is a state of the art technique for medical imaging using x-rays, with a broad range of applications. While CBCT systems for diagnostic and peri-interventional imaging, such as the Philips Allura FD20 (Philips Healthcare, Best, the Netherlands), can produce images with excellent spatial resolution, the contrast resolution is still somewhat inferior in comparison with other imaging techniques, such as traditional (fan beam) CT and magnetic resonance imaging (MRI) (Söderman et al., 2008) (Janssen and Hoff, 2012). The low contrast resolution results in a less distinctive visualization of the brain tissue, which can limit the diagnostic applications of CBCT systems. The relatively low contrast resolution of the images created with CBCT systems is due to the effects of scatter radiation (among other effects). Researchers have investigated several promising methods to enhance the contrast resolution, by implementing fast and accurate correction techniques for scatter radiation. The enhanced image quality is often physically assessed using phantoms, for example by Maher, Gao and Baer (Maher and Malone, 1997) (Gao et al., 2010) (Baer and Kachelrieß, 2012) (among others).

The phantoms that were used can generally be categorized as simple geometry phantoms or as anthropomorphic phantoms. Simple geometry phantoms such as the Catphan 600 (the phantom laboratory, Salem, New York, USA) are often equipped with low contrast and spatial resolution inserts for quantitative image quality assessment (IQA), but the scatter characteristics of such phantoms are not representative due to the shape of the phantom. Anthropomorphic phantoms represent anatomical features of the human head and are constructed using tissue equivalent materials (TEMs) and are therefore more likely to have realistic attenuation characteristics. Unfortunately, a limited range of commercial anthropomorphic head phantoms is available and these phantoms have certain limitations. For example, the commonly used Rando Alderson (Radiology Support Devices, Carson, California, USA) phantom is composed of TEMs that show an underattenuation (in terms of Hounsfield Units) in the lower diagnostic energy range of the x-ray photons (Shrimpton et al., 1981), which can result in a biased interpretation of the (enhanced) image quality. Also, along with other anthropomorphic phantoms, such as the ACS (Kyoto Kagaku, Kyoto, Japan) and the Atom Max (Computerized Imaging Reference systems inc, Norfolk, Virginia, USA), these phantoms lack inserts for the measurement of the contrast and spatial resolution of the image. Some researchers have ordered modified commercial phantoms (Sisniega et al., 2015) or even con-

*Corresponding author.
E-mail address: yichaowang1991@gmail.com (Y. Wang)

structed new phantoms, by adding inserts for low contrast resolution (Chiarot et al., 2005), but modified phantoms are relatively expensive and limit the accessibility for wide usage. Furthermore, while scatter radiation is an important factor in the interaction between the x-ray photons and the matter these photons pass through, the scatter characteristics of the TEMs are hardly investigated. Geraldelli (Geraldelli et al., 2013) has investigated the scatter characteristics of several TEMs including adipose, muscle and bone equivalent materials and Kozanetzky (Kozanetzky et al., 1987) has investigated the scatter characteristics of some plastic materials, but these studies only reported on the coherent scattering characteristics for a specific scattering angle, while incoherent scatter also contributes in the interaction between the x-ray photons and matter in the lower diagnostic energy range and it is of interest to know the spatial distribution of scatter radiation for IQA purposes. It is therefore of interest to address the shortcomings of the previously mentioned issues, by developing an anthropomorphic phantom which is (1) suitable for quantitative image quality assessment, (2) has materials with representative attenuation (both radiodensity and scatter) characteristics and (3) is suitable for cost-efficient 'home made' fabrication techniques for a wider accessibility.

This study reports on the design of such a phantom, where a selection of bone, muscle and brain equivalent materials were evaluated for their radiodensity, scatter characteristics and practical aspects for fabrication of a prototype using silicone casting and 3D printing were investigated.

2. Method & Materials

2.1. CBCT-data based design of the phantom

The design of the phantom was based on a 3D model of the human head, obtained from anonymous CBCT data of a male, similar to the methodology used by Kim (Kim et al., 2006). The data (DICOM format) for this study were obtained from a head XperCT protocol (Allura FD20, Philips Healthcare, Best, the Netherlands) and manually segmented into a skull mesh and into a soft tissue outer shell mesh (STL format) (figure 1) by adjusting the threshold of the intensity of the CBCT image using a customly developed tool at Philips Healthcare (AixiaViewer, D. Ruijters, Philips Healthcare, Best, the Netherlands). The STL meshes were post-processed using a mesh editing program (Blender, Amsterdam, the Netherlands), by manually closing holes in the maxillofacial region of the skull and by increasing the thickness of this region in order to increase the mechanical strength of the area. The skull was divided into three horizontally cut sections (the calvaria, maxilla and mandible) (figure 1a and b). Cylindrical (low) contrast inserts were positioned at the posterior area of the cranial cavity and a model of the ventricles, containing cerebrospinal fluid, was manually positioned within the cranial cavity (figure 1a to c). The 'muscle tissue' shell was divided into two vertically cut sections (figure 1 d). There was no design of the brain needed since the brain equivalent material of the phantom is a polymer-based gel (see section 2.2).

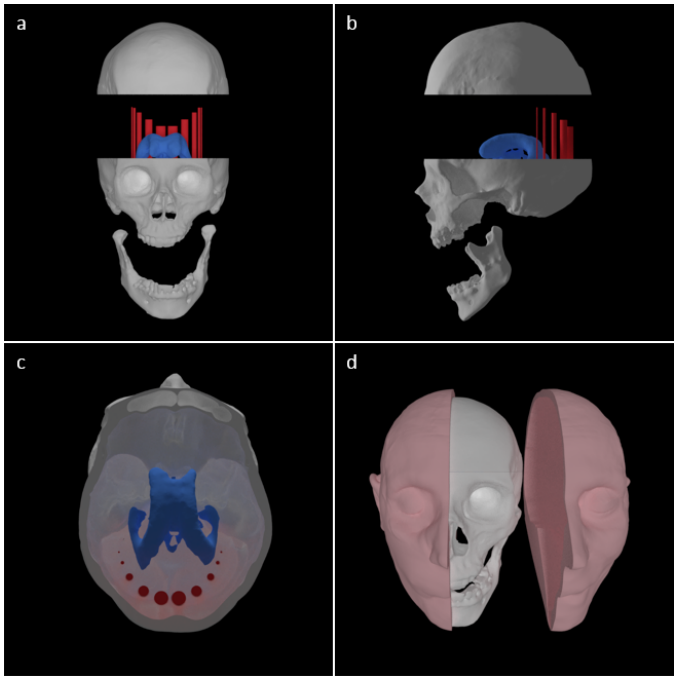

Figure 1: CBCT data based design a) anterior-posterior view of the skull mesh, containing inserts (red) and ventricles containing cerebrospinal fluid (blue). b) left lateral view of the skull mesh c) axial superior-inferior view of the skull mesh (no calvaria) with the low contrast inserts at the posterior side of the skull (red) and the ventricles (blue). d) vertically cut muscle shell mesh, surrounding the skull mesh.

2.2. Tissue equivalent materials

In previous studies, several researchers have investigated materials for the suitability as TEM for radiological purposes, including for dosimetry and for the construction of phantoms. These materials were often compared with human tissues in terms of mass attenuation coefficient (μ_m). Recommended bone equivalent materials include 'B-100' bone equivalent plastic and poly-vinylchloride (Akhlaghi et al., 2015), a dolomite-PMMA resin mixture (Ximenes et al., 2015), a dipotassium phosphate based mixture (Gallas et al., 2015) and a custom epoxy-resin based mixture (Jones et al., 2003). Recommended muscle equivalent materials include nylon (Mann et al., 2012), water (Poletti et al., 2004) (Geraldelli et al., 2013) and custom epoxy resin based mixtures, including 'Rando Alderson soft tissue equivalents' (Chiarot et al., 2005) and an Araldite-based mixture (Jones et al., 2003) (for a pediatric phantom).

Because the majority of the recommended TEMs were evaluated for usage in dosimetry and because not all of these materials were suitable for the specified 'home made' fabrication techniques (e.g. silicone casting and 3D printing), only nylon was considered as potential muscle equivalent material and selected for further evaluation in this study. Two novel TEMs for bone tissue and brain tissue are also proposed in this study, which are a mixture of monocalcium phosphate (MCPH) ($Ca(H_2PO_4)_2$), calcium sulfate ($CaSO_4$) and water (referred to as 'MCPHG') as bone equivalent material (3.85 wt% MCPH, 60 wt% $CaSO_4$ and 36.15 wt% water respectively) and a commercially available silyl-modified polymer gel (SMP) (Bison Polymax Crystal,

Table 1: Mass attenuation coefficient (μ_m) at 60, 80, 100 and 150 keV and physical density (ρ) of proposed tissue equivalent materials (TEMs) (Berger et al., 1998; ICRU, 1989) .

Tissue/TEM	$\mu_m(60keV)$	$\mu_m(80keV)$	$\mu_m(100keV)$	$\mu_m(150keV)$	$\rho\ [g/cm^3]$
Bone	0.315	0.222	0.186	0.148	1.92
Muscle	0.205	0.182	0.169	0.149	1.05
Brain	0.206	0.183	0.17	0.15	1.05
CSF/water	0.206	0.184	0.171	0.151	1.00
MCPHG	0.314	0.223	0.187	0.149	2.3
Nylon (PA12)	0.195	0.179	0.169	0.150	1.01
SMP	0.248	0.196	0.173	0.145	1.05

Bolton adhesives, Rotterdam, the Netherlands) as brain equivalent material. The mass attenuation coefficient (μ_m) of the TEMs were obtained from the online photon cross section database XCOM (Berger et al., 1998)), provided by the National Institute of Standards and Technology (NIST). The μ_m of the tissues and the physical density (ρ) were obtained from the International Commission on Radiation Units and Measurements (ICRU) report 44 (ICRU, 1989) and presented in table 1.

2.3. Evaluation of the radiodensity

The theoretical radiodensity of the TEMs were calculated using the linear attenuation coefficient (μ_x), by multiplying the mass attenuation coefficient of the TEMs with the physical density (ρ) of the TEM from table 1 (equation 1). Then the radiodensity in [HU] was then calculated using equation 2.

$$\mu_x = \mu_m \rho \tag{1}$$

Where μ_x is the linear attenuation coefficient of the TEM and ρ is the physical density of the TEM.

$$HU = 1000 \frac{\mu_x - \mu_{water}}{\mu_{water}} \tag{2}$$

Where μ_x and μ_{water} are the linear attenuation coefficient of the TEM and water respectively.

A Philips Allura FD20 x-ray system (Philips Healthcare, Best, the Netherlands) was used to measure the radiodensity of the TEM samples. The TEM samples were placed at the head side of the patient table (Maquet holding B.V. & Co. KG, Rastatt, Germany) along with a calibration phantom with known HU values (QRM-2DMC, QRM, Moehrendorf, Germany). A Head XperCT low dose, fast acquisition protocol was performed (at 120 kVp) for the acquisition of the 3D reconstructed image of each TEM. The image data were stored in DICOM format and analyzed using a computer tool for the measurement of HU values (DviewX, P. van der Haar, Philips Healthcare, Best, the Netherlands).

The median HU value and inter quartile range (IQR) of each TEM were calculated after manually assessing the HU value at 10 points at three different slices of the 3D volume.

The calibration phantom was used to check for a bias in the measured HU values of the TEM samples and to check for scaling effects and non-linearities of the HU scale. The results of the (calibration) measurements are presented in section 3.1 of the results.

2.4. Evaluation of the scatter characteristics

The same Allura FD20 x-ray system as the one for the radiodensity measurements was used to measure the scatter characteristics of the proposed TEMs. A modified version of the edge spread technique for scatter quantification (Cooper et al., 2000) was used, by positioning a lead plate 200 mm in front of the flat detector of the Allura (after removal of the anti-scatter grid) in order to block the top side of the incident x-ray beam. The three remaining sides were blocked using built in collimators at the source side of the x-ray system, so only the TEM would be radiated. TEM samples of 20 mm, 40 m and 60 mm thickness (100 x 100 mm width and height) were positioned behind the lead plate, 100 mm from the detector and 15 fluoroscopic images (in order to reduce the image noise) were taken at 60, 80, 100 and 120 kVp (at 100 mA) per TEM sample. The x-ray source to detector distance was 1200 mm. The photons of the incident x-ray beam that pass through the TEM sample are partially scattered and these scattered photons fall on the region of the flat detector behind the lead plate (figure 2).

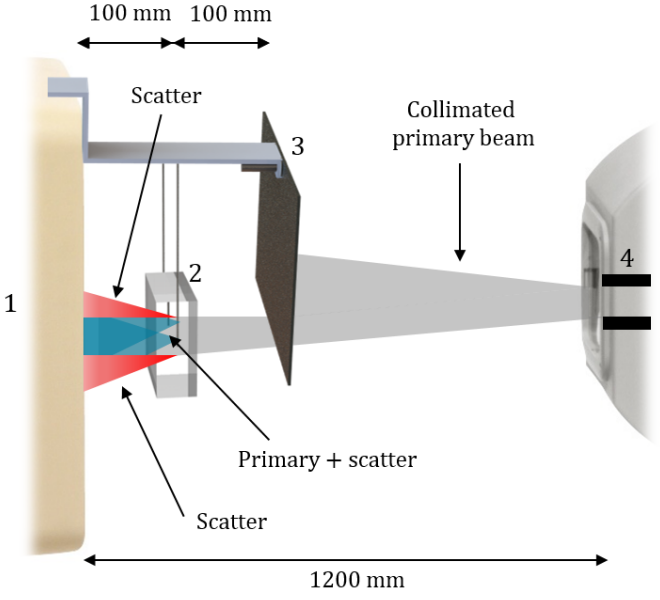

Figure 2: Experimental setup for the scatter measurements. The Philips Allura FD20 was used for a modified version of the edge spread technique (Cooper et al., 2000), by removing the anti-scatter grid from the flat detector (1) and positioning a TEM sample (2) between the lead plate (3) and detector. The x-ray beam is collimated at the source side (4).

Analysis of the intensity along a vertical pixel line at the center of the detector (in portrait mode) results in a characteristic intensity function, called the edge spread function (ESF), which is a function of the pixel position (x) on the detector (figure 3). The scatter characteristics of the TEMs, obtained by processing of the mean ESF (from the 15 fluoroscopic images), were defined in terms of scatter magnitude and spatial scatter distribution. The scatter magnitude was further defined as the maximal scatter to primary ratio (MSPR) of the TEM (equation 3) and the scatter magnitude at the edge of the lead plate (EM) (equation 4). The spatial scatter distribution (SD) was quantified as the pixel position behind the lead plate where the normalized scatter intensity reached 0.02 (figure 3). The value of 0.02 was selected because this point of the scatter function was most distinctive for each TEM with different thickness.

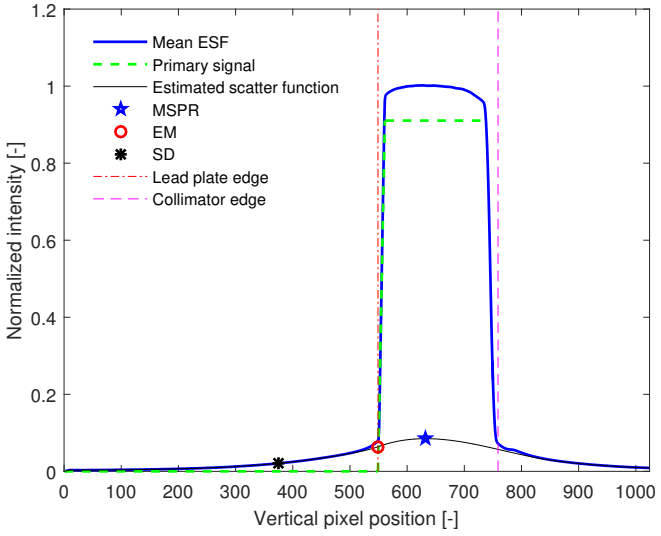

Figure 3: Example of the mean ESF and scatter function for one measurement (PMMA 40 mm at 120 kVp), where the SD and EM are measured and where the MSPR is estimated. The scatter function at the primary plus scatter region is estimated with a spline interpolation between the two measured scatter fractions at the edges of the lead plate and collimator.

$$MSPR = \frac{max(S(x))}{P(x)} \tag{3}$$

Where S(x) is the scatter function as a function of the pixel position (x) on the detector, obtained from the ESF(x) and P(x) is the primary function after subtracting S(x) from the ESF(x).

$$EM = max(\frac{d^2 ESF(x)}{dx^2}) \tag{4}$$

The setup was calibrated to correct for the Heel effect and for veiling glare of the detector. The Heel effect, caused by the anode of the x-ray system, results in a gradient in the ESF and the effects of veiling glare on a flat detector can result in an overestimation of the scatter signal of up to 15% (Lazos and Williamson, 2012). The scatter function was estimated by applying a spline interpolation between the two scatter fractions behind the lead plate and the collimator, using the angles of the scatter fractions at the edge.

The experimental setup and data processing methodology were validated by comparing the physical measurements of polymethymethacrylate (PMMA) samples with Monte Carlo (MC) based scatter simulations of PMMA samples with the same thicknesses at the same tube voltages (figure 4). The MSPR, EM and SD ratios between the measurements and MC simulations for measurements at two different test labs were 0.87, 1.00, 1.00 and 1.03, 1.13, 0.96 (IQRs between 0.05 and 0.14) and therefore the experimental setup and estimation methodology were considered valid.

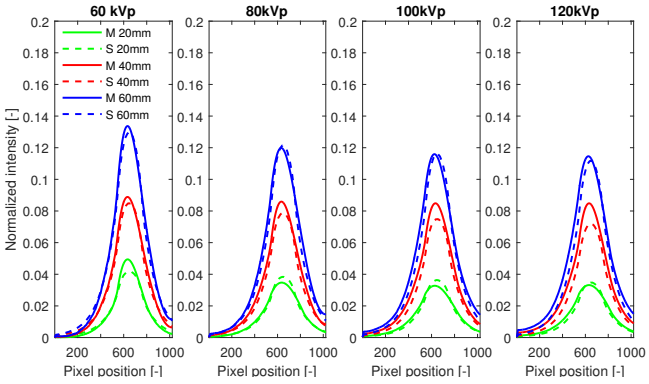

Figure 4: Comparison between the measured (M) and simulated (S) scatter functions of PMMA for 20, 40 and 60 mm at 60, 80, 100 and 120 kVp (100 mA).

After validation of the experimental setup, the scatter characteristics of the proposed MCPHG, nylon and SMP were compared to MC simulations of bone, muscle and brain tissue respectively. The results of the comparison can be found in section 3.2 of the results.

2.5. *Fabrication and evaluation of the prototype*

A prototype of the right anterior part of the designed phantom (figure 5a) was fabricated using the proposed TEMs and the practical aspects of the TEMs for actual usage for the construction of the phantom and imaging aspects (e.g. anatomical structures or image artifacts) of the prototype were compared with the CBCT data of the anonymous head. Feedback from experts in x-ray and CT image quality was used in order to verify the usability of the phantom.

The MCPHG skull was fabricated using silicone casting (shore 15 silicone casting rubber, Polyestershoppen B.V., Moordrecht, the Netherlands), where a positive mold of the skull (two pieces) was fabricated using FDM printing (Ultimaker 2, Geldermalsen, the Netherlands) at the student workshop of the faculty of mechanical, maritime and materials engineering at Delft university of technology (figure 5b and c). The initially liquid MCPHG was stirred with intervals for approximately one hour in order to remove air bubbles that emerged during the hardening of the mixture, before being poured into the cast. The SMP-gel was injected into the cranial cavity of the skull using a silicone kit injector and the muscle shell was fabricated using selective laser sintering of nylon powder (modified polyamide 12 powder) (Shapeways, Eindhoven, the Netherlands) (figure 5d).

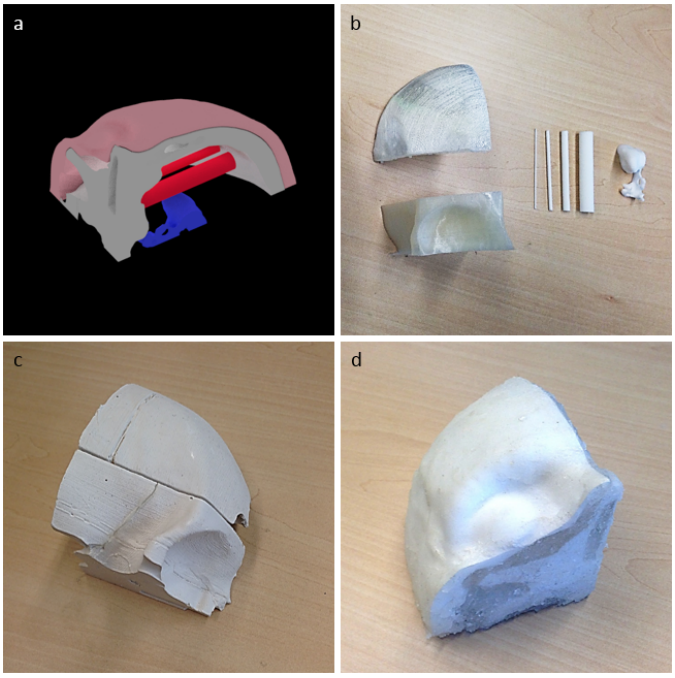

Figure 5: Prototype of the right anterior part of the design. a) STL model of the muscle shell (pink), skull (grey), low contrast inserts (red) and ventricle (blue). b) 3D printed skull mold and insert parts. c) MCPHG skull. d) finished prototype with nylon muscle shell and the SMP injected into the cranial cavity.

3. Results

3.1. Radiodensity of the TEMs

The calculated and measured HU values of MCPHG, nylon and SMP after calibration are visualized in figure 6 and summarized in table 2.

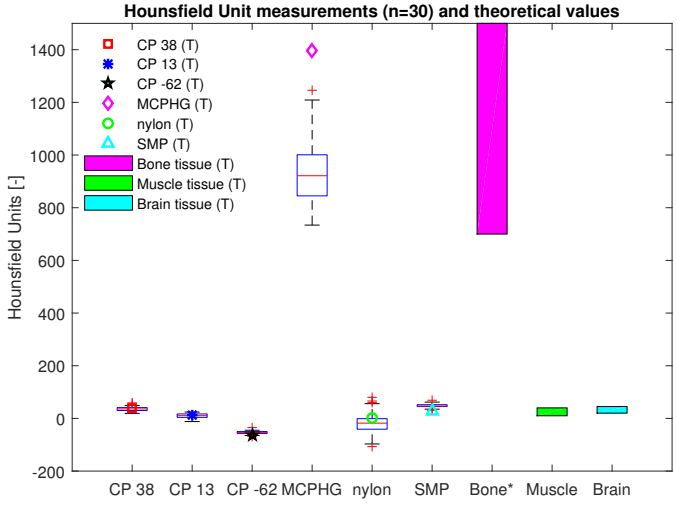

Figure 6: Summary plot of measured and theoretical (T) HU values for the calibration phantom (CP), MCPHG, nylon and SMP. The theoretical HU range of the tissues (Ali and Ray, 2013) are also plotted for comparison. *Please note that the HU range of bone goes up to 3000 (not shown in this figure).

3.2. Scatter characteristics of the TEMs

The measured MSPR, EM and SD of MCPHG, nylon and SMP are plotted along MC simulations of bone, muscle and brain tissues in figure 7 to 9 respectively.

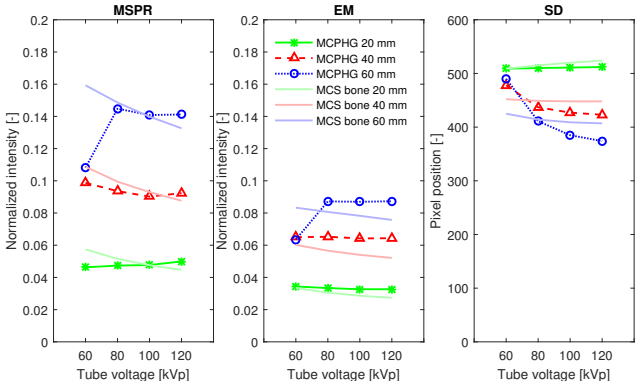

Figure 7: Summary plot of the ratio between the measurement and MC simulation (MCS) of MCPHG versus bone tissue.

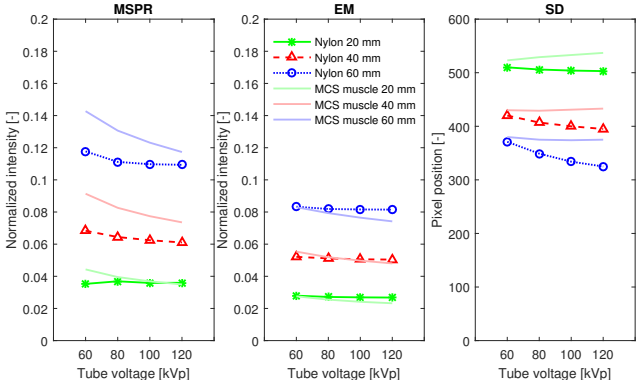

Figure 8: Summary plot of the ratio between the measurement and MC simulation (MCS) of nylon versus muscle tissue.

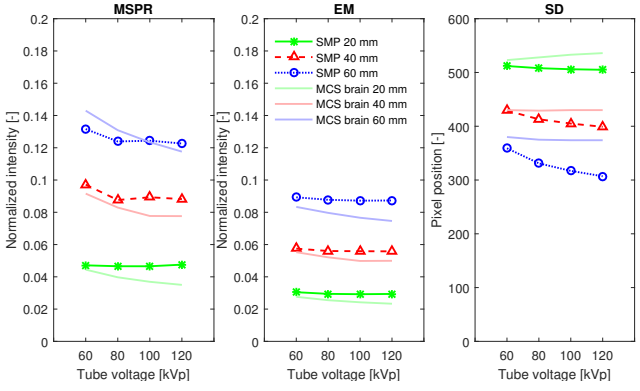

Figure 9: Summary plot of the ratio between the measurement and MC simulation (MCS) of SMP versus brain tissue.

From these figures it can be seen that the overall scatter characteristics of the proposed TEMs are in good agreement with the simulated tissues, except for the MSPR, EM and SD of the 60

Table 2: The median, 25th percentile (Q1), 75th percentile (Q3) of the measured HU values for the calibration phantom (CP), and TEMs are summarized along with the calculated HU values using equation2 of the CP and TEMs and along the theoretical HU range of tissues (Ali and Ray, 2013).

Material	Median (n=30)	Q1	Q3	Theoretical HU value	Tissue HU range
CP 38	36	30	41	38	-
CP 13	11	4	17	13	-
CP -62	-54	-57	-50	-62	-
MCPHG	922	845	1001	1398	700-3000 (bone)
Nylon	-18	-41	-1	1	5-40 (muscle)
SMP	47	45	52	27	20-45 (brain)

mm MCPHPG sample at 60 kVp, which are significantly lower in comparison with the MC simulation of bone tissue. After analysis of the estimated scatter function for this measurement, an inaccurate estimation of the scatter function was observed due to a large presence of noise signals on the detector. It was therefore considered acceptable to exclude this measurements from the overall results. A summary of the MSPR, EM and SD ratios between the measured TEMs and simulated tissues are can be found in table 3

Table 3: Summary of the median (Mdn) ratios and inter quartile range (IQR) between the measured TEMs and simulated tissues.

Material/ tissue	MSPR ratio (n=12)		EM ratio (n=12)		SD ratio (n=12)	
	Mdn	IQR	Mdn	IQR	Mdn	IQR
MCPHG/bone	0.95	0.13	1.13	0.10	0.98	0.05
Nylon/muscle	0.84	0.13	1.04	0.07	0.94	0.05
SMP/brain	1.06	0.14	1.12	0.07	0.94	0.06

3.3. Qualitative evaluation of the prototype

From a qualitative comparison between the CBCT patient data and the constructed prototype (figure 10), several remarkable observations could be made. A significant difference was observed between the the structure of the skull from the patient data and the MCPHG skull. Real bone tissue in the skull is composed of cortical bone at the outer layers and trabecular bone between these layers and is therefore more radiodense at the outer layers in comparison with the center. The MCPHG skull showed a more homogeneous representation of the skull, although some minor differences in radiodensity were observed between the surface and the center of the MCPHG skull (figure 10 d), where the surface appeared to be more radiodense in comparison with the center. Another remarkable observation that was made was the presence of some relatively big air pockets within different areas of the prototype, especially at the region of the SMP, which represents the brain tissue (figure 10 f). The inserts for the measurement of the contrast resolution and ventricles were visible and useful on all relevant patient views of the images (i.e. anterior-posterior, lateral and axial view).

4. Discussion and recommendations

In this study, a head phantom was designed for quantitative IQA in CBCT. This design was made in order to solve several issues of existing commercial head phantoms for IQA in CBCT, including an underattenuation of the materials in the lower diagnostic energy range, the lack of inserts for quantitative IQA and the relatively high costs of most of the phantoms. The current design is equipped with inserts for quanatitative measurement of the contrast resolution and composed of TEMs that are suitable for simple 'home made' fabrication techniques. The TEMs were quantitatively evaluated in terms of radiodensity, scatter characteristics and qualitatively evaluated in terms of the suitability for simple fabrication techniques and the presence of image artifacts.

The radiodensity of MCPHG and SMP were considered representative as bone and brain tissue respectively, since the measured median HU values were within the theoretical range HU values of bone and brain tissue. The median HU values of nylon were out of the range of the HU values for muscle tissue, but in the design of the outer muscle shell of the prototype, no adipose tissue was included. If adipose tissue were to be included into the muscle shell, the average HU value would be lower, because the theoretical HU value of adipose tissue varies between -100 and -50 (Ali and Ray, 2013). Since adipose tissue is present in the outer layers of the human head, it is reasonable to consider nylon as a representative 'soft tissue' equivalent material, to be used in the outer shell of the phantom. However, the scatter characteristics of adipose tissue were not taken into account in this study and should be included in the comparison in future work.

The median MSPR, EM and SD ratios between the measured TEMs and simulated tissues ranged from 0.84 to 1.13 and the IQR ranged from 0.05 to 0.14. By looking at the absolute difference in the normalized MSPR and EM signal, this means that the largest difference between the TEMs and simulated tissues was less than 3 percent. It is therefore reasonable to say that the proposed TEMs are representative as bone, muscle and brain equivalent materials, in terms of scatter characteristics.

The method for the quantification of the scatter characteristics was verified by comparing measurements of PMMA with Monte Carlo based scatter simulations of PMMA. While the verification was performed for multiple thicknesses at multiple tube voltages, the sample size was still considered too small for performing a sensitivity analysis about the accuracy and reliability of the measurements. It is recommended to perform the verification with a more diverse selections of materials in order to be able to draw conclusions about the accuracy and reliability of the measurements using this method.

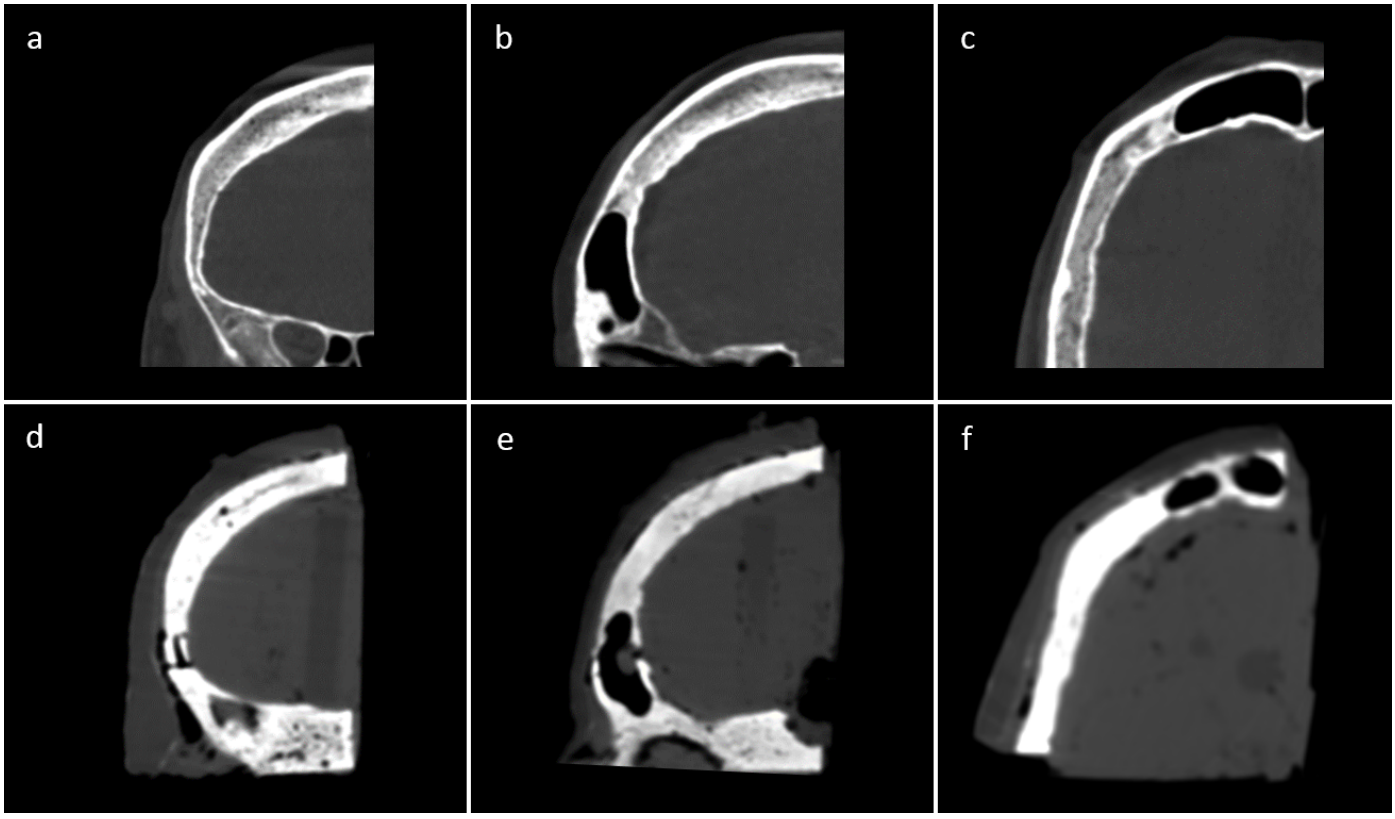

Figure 10: Comparison between the CBCT data of the anonymous patient head (a to c) and the prototype of the phantom with inserts for quantitative measurement of the contrast resolution (d to f). a and d: anterior-posterior view. b and e: left lateral view c and f: axial inferior-superior view. The inserts are visible in all relevant views and can be used for quantitative evaluation of the contrast resolution of the image.

While the scatter characteristics of the proposed TEMs were considered as representative for tissues in the head, more materials can be investigated using this technique, for example to find materials that have even better matching attenuation characteristics or are easier to work with. It is suggested to investigate the attenuation characteristics of calcium rich powders that are suitable for 3D printing, including monocalcium phosphate powder, which was used in this study, since researchers in the field of regenerative medicine have already shown that these calcium rich powders can be used to create durable and accurate scaffolds using 3D printing techniques, so this technique could be applied for the fabrication of the skull.

Based on the qualitative evaluation of the prototype, several improvements are needed in future work. Especially the injection of the SMP into the cranial cavity should be carefully done, in order to minimize the amount of trapped air. Preliminary tests for injection using a wider nozzle show that it is possible to inject the SMP with nearly no air. Furthermore, a complete phantom should be fabricated and tested in order to demonstrate that the approach from this study can be applied in practice.

5. Conclusions

The goal of this study was to investigate the feasibility of fabricating an anthropomorphic head phantom for quantitative image quality assessment in CT and/or CBCT, with representative attenuation characteristics and inserts for the measurement of the contrast resolution. A prototype was fabricated using newly introduced TEMs which are suitable for 'home made' fabrication techniques such as silicone casting and 3D printing. The measured radiodensity of the TEMs were in agreement with the radiodensity of the tissues that these TEMs should resemble and the scatter characteristics of the TEMs were evaluated and found to be representative as well. The design is suitable for simple fabrication techniques such as silicone rubber casting and 3D printing, which makes this phantom a potential alternative for researchers who want to fabricate their own phantom at low costs.

6. Acknowledgments

This study was funded by the innovation department of image guided therapy systems at Philips Healthcare, Best, the Netherlands. The author would like to thank D. Ruijters and P. van der Haar from Philips Healthcare for their expert opinion regarding the usability of the prototype, M. Pieters for the Monte Carlo based scatter simulations and de Bron B.V. for kindly sponsoring of the monocalcium phosphate powder.

7. Conflict of interest

The author declares that he has no conflict of interest.

References

Akhlaghi, P., Miri Hakimabad, H., Rafat Motavalli, L., 2015. Determination of tissue equivalent materials of a physical 8-year-old phantom for use in computed tomography. Radiation Physics and Chemistry 112, 169–176.
URL: http://dx.doi.org/10.1016/j.radphyschem.2015.03.030
DOI: 10.1016/j.radphyschem.2015.03.030

Ali, M. F., Ray, S., 2013. SAR analysis for handheld mobile phone using DICOM based voxel model. Journal of Microwaves, Optoelectronics and Electromagnetic Applications 12 (2), 363–375.
DOI: 10.1590/S2179-10742013000200010

Baer, M., Kachelrieß, M., 2012. Hybrid scatter correction for CT imaging. Physics in Medicine and Biology 57 (21), 6849–6867.
DOI: 10.1088/0031-9155/57/21/6849

Berger, M., Hubbell, J., Seltzer, S., Chang, J., Coursey, J., Sukumar, R., Zucker, D., Olsen, K., 1998. XCOM: Photon Cross Sections Database.
URL: http://physics.nist.gov/PhysRefData/Xcom/Text/version.shtml

Chiarot, C. B., Siewerdsen, J. H., Haycocks, T., Moseley, D. J., Jaffray, D. A., 2005. An innovative phantom for quantitative and qualitative investigation of advanced x-ray imaging technologies. Physics in Medicine and Biology 50 (21), N287–N297.
DOI: 10.1088/0031-9155/50/21/N01

Cooper, V. N., Boone, J. M., Seibert, J. a., Pellot-Barakat, C. J., 2000. An edge spread technique for measurement of the scatter-to-primary ratio in mammography. Medical physics 27 (5), 845–853.
DOI: 10.1118/1.598950

Gallas, R. R., Hünemohr, N., Runz, A., Niebuhr, N. I., Jäkel, O., Greilich, S., 2015. An anthropomorphic multimodality (CT/MRI) head phantom prototype for end-to-end tests in ion radiotherapy. Zeitschrift fur Medizinische Physik 25 (4), 391–399.
URL: http://dx.doi.org/10.1016/j.zemedi.2015.05.003
DOI: 10.1016/j.zemedi.2015.05.003

Gao, H., Fahrig, R., Bennett, N. R., Sun, M., Star-Lack, J., Zhu, L., 2010. Scatter correction method for x-ray CT using primary modulation: phantom studies. Medical Physics 37 (12), 934–946.
URL: http://www.ncbi.nlm.nih.gov/entrez/query.fcgi?cmd=Retrieve{&}db=PubMed{&}dopt=Citation{&}list{_}uids=20229902
DOI: 10.1118/1.3298014

Geraldelli, W., Tomal, A., Poletti, M. E., 2013. Characterization of tissue-equivalent materials through measurements of the linear attenuation coefficient and scattering profiles obtained With Polyenergetic Beams. IEEE Transactions on Nuclear Science 60 (2), 566–571.
DOI: 10.1109/TNS.2013.2248382

ICRU, 1989. Tissue substitutes in radiation dosimetry and measurement (report 44). Tech. rep., Bethesda, MD.

Janssen, P. M., Hoff, E. I., 2012. Teaching NeuroImages: Subacute intracerebral hemorrhage mimicking brain tumor. Neurology 79 (21), e183.
URL: http://www.ncbi.nlm.nih.gov/pubmed/23170017
DOI: 10.1212/WNL.0b013e3182752cfd

Jones, A. K., Hintenlang, D. E., Bolch, W. E., 2003. Tissue-equivalent materials for construction of tomographic dosimetry phantoms in pediatric radiology. Medical physics 30 (8), 2072–2081.
DOI: 10.1118/1.1592641

Kim, J. I., Choi, H., Lee, B. I., Lim, Y. K., Kim, C. S., Lee, J. K., Lee, C., 2006. Physical phantom of typical Korean male for radiation protection purpose. Radiation Protection Dosimetry 118 (1), 131–136.
DOI: 10.1093/rpd/nci338

Kozanetzky, J., Knoerr, B., Harding, G., Neitzel, U., 1987. X-ray diffraction measurements of some plastic materials and body tissues. Medical Physics 14, 526–532.
DOI: 10.1118/1.596143

Lazos, D., Williamson, J. F., 2012. Impact of flat panel-imager veiling glare on scatter-estimation accuracy and image quality of a commercial on-board cone-beam CT imaging system. Medical Physics 39 (9), 5639.
DOI: 10.1118/1.4747260

Maher, K. P., Malone, J. F., 1997. Computerized scatter correction in diagnostic radiology. Contemporary Physics 38 (2), 131–148.
URL: http://www.tandfonline.com/doi/abs/10.1080/001075197182469
DOI: 10.1080/001075197182469

Mann, K. S., Kurudirek, M., Sidhu, G. S., 2012. Verification of dosimetric materials to be used as tissue-substitutes in radiological diagnosis. Applied Radiation and Isotopes 70 (4), 681–691.
URL: http://dx.doi.org/10.1016/j.apradiso.2011.12.008
DOI: 10.1016/j.apradiso.2011.12.008

Poletti, M. E., Gonçalves, O. D., Mazzaro, I., 2004. Measurements of X-ray scatter signatures for some tissue-equivalent materials. Nuclear Instruments and Methods in Physics Research, Section B: Beam Interactions with Materials and Atoms 213, 595–598.
DOI: 10.1016/S0168-583X(03)01676-8

Shrimpton, P. C., Wall, B. F., Fisher, E. S., 1981. The tissue-equivalence of the Alderson Rando anthropomorphic phantom for x-rays of diagnostic qualities. Physics in medicine and biology 26 (1), 133–139.
DOI: 10.1088/0031-9155/26/1/013

Sisniega, A., Zbijewski, W., Xu, J., Dang, H., Stayman, J. W., Yorkston, J., Aygun, N., Koliatsos, V., Siewerdsen, J. H., 2015. High-fidelity artifact correction for cone-beam CT imaging of the brain. Physics in Medicine and Biology 60 (4), 1415–1439.
URL: http://stacks.iop.org/0031-9155/60/i=4/a=1415
DOI: 10.1088/0031-9155/60/4/1415

Söderman, M., Babic, D., Holmin, S., Andersson, T., 2008. Brain imaging with a flat detector C-arm: Technique and clinical interest of XperCT. Neuroradiology 50 (10), 863–868.
DOI: 10.1007/s00234-008-0419-1

Ximenes, R. E., Silva, A., Balbino, D., Poletti, M. E., Maia, A. F., 2015. Development of an anthropomorphic head phantom using dolomite and polymethyl methacrylate for dosimetry in computed tomography. Radiation Physics and Chemistry 117, 203–208.
URL: http://dx.doi.org/10.1016/j.radphyschem.2015.08.019
DOI: 10.1016/j.radphyschem.2015.08.019